Biosensors and Bioelectronics 154 (2020) 112014

Contents lists available at ScienceDirect

Biosensors and Bioelectronics

journal homepage: http://www.elsevier.com/locate/bios

An enzyme-free and substrate-free electrochemical biosensor with robust porphyrin-based covalent-linked nanomaterial as nanoelectrocatalyst and efficient support for sensitive detection of uracil-DNA glycosylase

Tingting Liu [a], Lin Cui [b,*], Dekang Li [a], Wenqiang Gao [a], Lili Wu [c], Xiaomei Zhang [a,**]

[a] School of Chemistry and Chemical Engineering, Shandong University, Jinan, Shandong, 250100, China
[b] College of Chemistry, Chemical Engineering and Materials Science, Shandong Normal University, Jinan, Shandong, 250014, China
[c] School of Materials Science and Engineering, Shandong University, Jinan, Shandong, 250100, China

ARTICLE INFO

Keywords:
Electrochemical biosensor
Uracil DNA glycosylase
Porphyrin
Electrocatalytic reduction
Substrate-free

ABSTRACT

We developed a novel electrochemical biosensor for uracil-DNA glycosylase (UDG) detection based on enzyme-free and substrate-free electrocatalytic signal amplification by porphyrin-based covalent-linked nanomaterial (OAPS-Por). This OAPS-Por could not only absorb much Thionine (Thi), but also possess obvious electrocatalytic activity toward the reduction of Thi without involvement of H_2O_2. Sequentially, the functionalized OAPS-Por with Thi, Au nanoparticles and single-stranded DNA (OAPS-Por/Thi@AuNPs-ssDNA) was ingeniously designed as the signal probe. Meantime, the hairpin DNA (hDNA) with four uracil bases was immobilized on AuNPs/GCE via an Au–S bond. When UDG was present, the uracil in hDNA was removed and hairpin structure was unfolded. Next, the signal probes binded with the unfolded hDNA by DNA hybridization. The Thi in signal probes could generated an original electrochemical signal, which could be further amplified and output due to the robust electrocatalytic activities of OAPS-Por toward Thi. As a result, the as-constructed electrochemical biosensor had a broad linear range from 0.005 to 1 U mL^{-1}. It also exhibited a low detection limit of 6.97×10^{-4} U mL^{-1}. Moreover, this biosensor could be used to assay the inhibition of UDG (UGI) and the UDG activity in real samples (HeLa cell lysates and human blood serums), and demonstrated great prospect in clinical diagnostics and biomedical research.

1. Introduction

Metalloporphyrin has been widely used as a mimetic enzyme to amplify the indication signal in electrochemical biosensors, due to its superior biocompatibility and high catalytic efficiency (Ling et al., 2015; Wang et al., 2013; Zheng et al., 2015). However, the catalytic activity of monomeric metalloporphyrin is weak, due to the self-degradation of the porphyrins and the formation of μ-oxide dimers (Xue et al., 2012). At present, the method immobilizing porphyrins into solid matrices was developed, which significantly improved the catalytic activity of porphyrin-based materials (Ling et al., 2016; Q. Liu et al., 2019).

Among them, porphyrin-based covalent-linked nanomaterials have attracted wide interest because of the low skeleton density, high stability, abundant active sites and effective protection of cofactors by immobilizing each porphyrin ligand at specific location. In addition, porphyrin-based covalent-linked nanomaterials can also act excellent supports for other functional molecules. Benefiting from these merits, such materials have been used in various applications including photocatalysis (Nagai et al., 2013), electrocatalysis (Wu et al., 2014; Xiang et al., 2014; Lin et al., 2015), catalytic oxidation (Chen et al., 2010) and biomimetic catalytic reactions (Wang et al., 2014). Compared with natural enzymes and porphyrin monomers, superior catalytic activity of porphyrin-based covalent-linked nanomaterials has been revealed. However, reports about such nanomaterial for electrochemical biosensor are still barren.

In addition, when artificial enzymes such as mimetic peroxidase was used as electrocatalysts, H_2O_2 was often used as the catalytic substrate. However, the unstable chemical property of H_2O_2 increases the uncertainty of operation and influences the sensitivity (Cui et al., 2019). Therefore, the investigation about stable substrate-free electrochemical

* Corresponding author.
** Corresponding author.
E-mail addresses: zpbzcl@126.com (L. Cui), zhangxiaomei@sdu.edu.cn (X. Zhang).

https://doi.org/10.1016/j.bios.2020.112014
Received 15 October 2019; Received in revised form 25 December 2019; Accepted 8 January 2020
Available online 10 January 2020

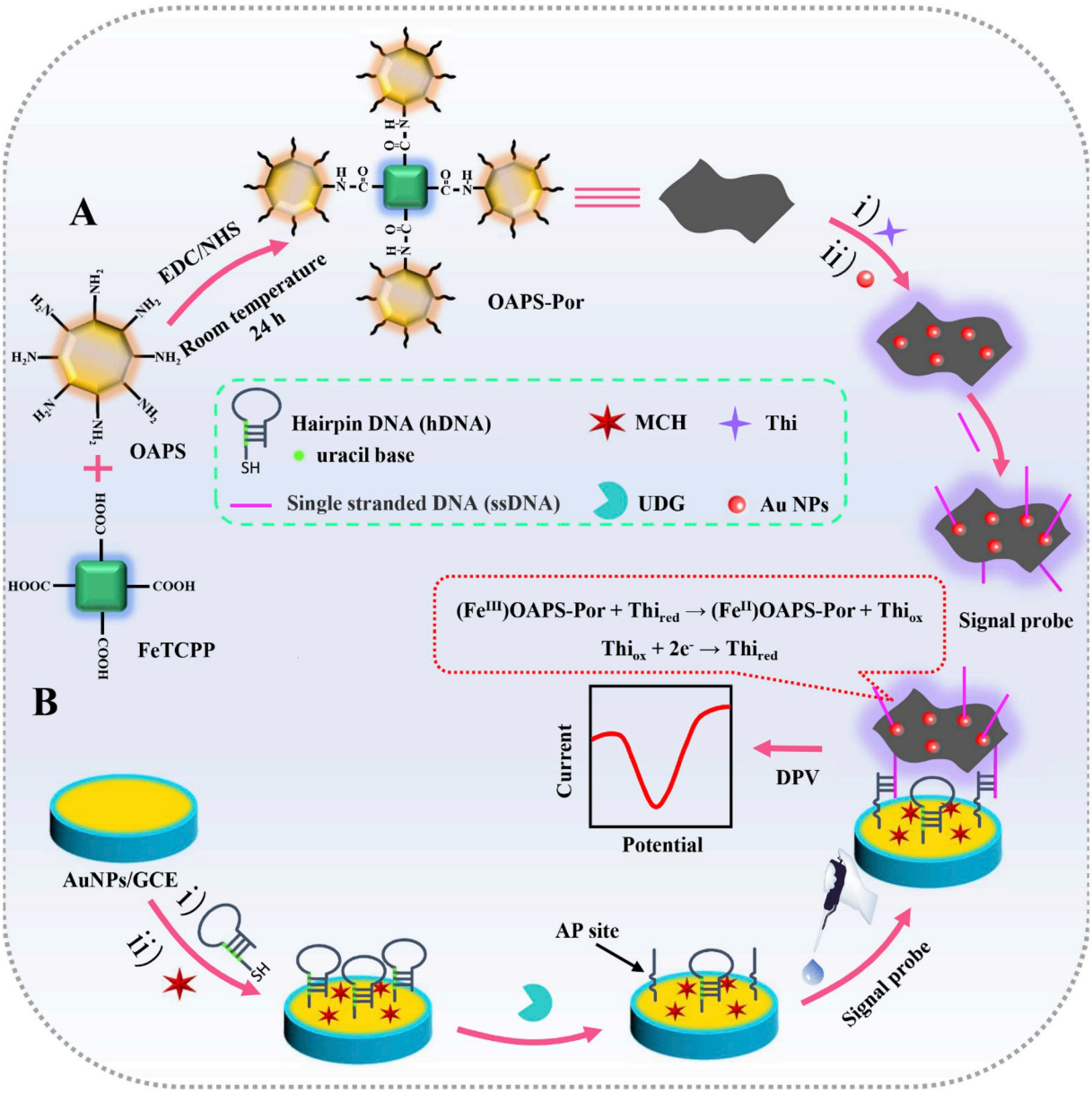

Scheme 1. Schematic representation of (A) the synthesis of OAPS-Por and (B) the sensing principle of the electrochemical detection of UDG.

biosensor is urgently needed. Yuan's group showed that L-cysteine can act as a stable catalytic substrate to induced manganese porphyrin electrocatalytic amplification in an electrochemical aptasensor for thrombin detection (Zheng et al., 2015). Zheng et al. discovered that the Fe_3O_4@Ag–Pd hybrid particle had excellent electrocatalytic activity toward small dye molecules without the involvement of H_2O_2, and could be used as a signal-amplifying nanoprobe to constructed an electrochemical cytosensor (Zheng et al., 2014). A small drawback of this cytosensing is that when the dye molecules are placed in the test solution, a higher background signal may result and affect the activity of biomolecules on the electrode. If the electroactive indicator molecule is loaded on nanomaterials, this problem will be solved.

The base excision repair (BER) is a common DNA repair mechanism. In this process, DNA glycosylases, such as uracil-DNA glycosylase (UDG), are essential in the maintenance of genome stability (David and Williams, 1998; David et al., 2007). With the help of UDG, the damaged uracil base in DNA was recognized and removed, generating an apurinic/apyrimidinic (AP) site (Schärer, 2003). It has reported that the abnormal UDG activity can resulted in various diseases, such as chemotherapy resistance (Tao et al., 2015), lymphoma (Sousa et al., 2007), and Bloom syndrome (Seal et al., 1988). Thus, rapid and sensitive detection of UDG activity is significant for clinical diagnostic researches.

Some methods for UDG assay have been developed, such as gel electrophoresis (Di Noia and Neuberger, 2002), autoradiography (Nc and Harris CCBohr, 2004), electrochemiluminescence (ECL) (T. Liu et al., 2019), and colorimetric assay (Du et al., 2016). Nevertheless, these methods suffered from sophisticated instruments, complicated operation, time-consuming procedure, and low sensitivity. To overcome these limitations, fluorescent methods were introduced for UDG activity assays due to its rapidity, simple operation, and high sensitivity (Li et al., 2018; Wang et al., 2017; Wei et al., 2018; Wu et al., 2015). However, fluorescent approaches usually need DNA probes labelled with pairs of fluorophores and quenchers, and suffer from high background signals when the quenching was incomplete. An electrochemical biosensor with the merits of fast response, desirable sensitivity, and simple operation attracted increasing attention in various biological sensing and was recently introduced in UDG detection (Jiao et al., 2016; Liu et al., 2013).

Based on these considerations, we designed a novel porphyrin-based

nanomaterial using octa (aminophenyl) silsesquioxane (OAPS) and Fe-Tetrakis (4-carboxyphenyl) porphyrin (FeTCPP), namely OAPS-Por, in Scheme 1A. OAPS is one of the polyhedral oligomeric silsesquioxane (POSS), which had eight 4-aminophenyl groups (Liao et al., 2014). Because their high solubility in many inorganic and organic solvents as well as attaching abundant $–NH_2$ groups, OAPS can serve as functionalized reaction sites, which enable the final OAPS-functionalized nanomaterials possessing good dispersibility in many organic and inorganic solvents (Ghanbari et al., 2011; Zhang et al., 2016). OAPS-Por can not only absorb much thionine (Thi) by π-π interaction, but also possess obvious electrocatalytic activity for Thi in the absence of H_2O_2. Based on this feature, an amplified-signal nanoprobe (OAPS-Por/-Thi@AuNPs-ssDNA) was proposed in the ultrasensitive electrochemical biosensor for UDG detection. The principle of the proposed strategy is shown in Scheme 1B. The hairpin DNA (hDNA) with four uracil bases was immobilized on AuNPs/GCE by an Au–S bond. When UDG was present, the uracil in hDNA was removed, leading to the release of single-stranded DNA. Then the signal probe OAPS-Por/Thi@AuNPs-ssDNA, fabricated from OAPS-Por/Thi@AuNPs and ssDNA, was introduced to the electrode surface by DNA hybridization. The OAPS-Por could not only load many redox molecules (Thi), but could also electrocatalyze the reduction of Thi making the electrochemical signal amplified without adding any unstable substrate such as H_2O_2. The fabricated electrochemical biosensor exhibited rapid, sensitive, and highly sensitive detection of UDG against other interferences.

2. Material and method

2.1. Materials and apparatus

All chemicals and related instruments involved in the experiments have been described in Supporting information.

2.2. Preparation of OAPS-Por and OAPS-Por/Thi

To activate the –COOH groups of FeTCPP, FeTCPP (52.75 mg, 0.0625 mM) was added into 100 mL EDC/NHS (EDC: 34 mM; NHS: 34 mM) hybrid solution and stirred at room temperature (R.T.) for 12 h. Then OAPS (36 mg, 0.03125 mM) was added into the above solution under stirring for another 24 h. Finally, gray-black powder was obtained via filtration and dried in under a 80 °C vacuum overnight for further use.

To obtain a OAPS-Por/Thi composite, OAPS-Por (40 mg) was dispersed into Thi solution (40 mL, 100 mg L^{-1}), followed by stirring at R.T. for 24 h to reach the adsorption equilibrium. The precipitate was isolated via filtration, washed with distilled water three times to remove loosely adsorbed Thi, and then dried at 80 °C under a vacuum for 24 h.

2.3. Preparation of OAPS-Por/Thi@AuNPs and OAPS-Por/Thi@AuNPs-ssDNA

For preparation of OAPS-Por/Thi@AuNPs, 2 mg OAPS-Por/Thi was added into the prepared AuNPs solution (Cui et al., 2018) (6 mL, pH 5.0, adjusted by citric acid-sodium citrate buffer solution) with magnetically stirring for 12 h at ambient temperature. The residual amino groups of OAPS bound to AuNPs by electrostatic force. The OAPS-Por/Thi@AuNPs was obtained by centrifugation at 6000 rpm, rinsed several times with water, and dispersed in Tris-HCl (1 mL, pH 7.4) solution.

OAPS-Por/Thi@AuNPs-ssDNA was prepared by the conjugation between –SH groups of DNA and AuNPs in OAPS-Por/Thi@AuNPs. The process was as follows: ssDNA (400 μL, 2 μM) was added into OAPS-Por/Thi@AuNPs solution and slightly stirred at 4 °C for 12 h. After rinsing three times with 10 mM Tris-HCl at 6000 rpm for 5 min to remove the excess DNA, OAPS-Por/Thi@AuNPs-ssDNA as a signal probe was redispersed in 1 mL Tris-HCl (10 mM) and left at 4 °C for further use.

2.4. Construction of the electrochemical sensing platform

To construct the electrochemical biosensor, a bare glassy carbon electrode (GCE) (d = 3 mm) was polished with 1.0, 0.3 and 0.05 μm Al_2O_3 powder on chamois leather and washed successively with water-ethanol-water for 5 min under sonification, followed by drying in nitrogen. To attach hDNA, the GCE was electrodeposited in 0.8% $HAuCl_4$ solution under -0.2 V for 30 s, obtaining AuNPs on GCE. Then 10 μL of annealed hDNA (0.5 μM) was connected on the modified electrode via an Au–S bond. After incubation overnight at 4 °C, the electrode was washed with 10 mM Tris solution (pH 7.4). After that, the hDNA/AuNPs/GCE was blocked with MCH (1 mM, 10 μL) at ambient temperature for 30 min. After washing, the MCH/hDNA/AuNPs/GCE electrode was obtained.

2.5. Analysis of UDG activity and UDG inhibition

To detect UDG activity, 10 μL of reaction solution containing 1 μL of 10 × UDG reaction buffer (200 mM Tris-HCl, 10 mM EDTA, 10 mM DTT, pH 8.0) and various concentrations of UDG was dropped on the MCH/hDNA/AuNPs/GCE electrode at 37 °C for 60 min. Then, the electrode was immersed with 10 μL of OAPS-Por/Thi@AuNPs-ssDNA at 37 °C for 1 h. Ultimately, the electrode determined differential pulsevoltammograms (DPV) after rinsing with pH 7.4 Tris-HCl. DPV was recorded in 0.1 M HAc-NaAc (pH 5.0) from 0.2 to -0.5 V with 50 mV modulation amplitude.

UDG inhibition was also investigated and UGI was selected as a model inhibitor. The specific process was as follows: first, 5 μL of various concentrations of UGI containing 0.5 μL of 10 × UDG reaction buffer was dropped onto the MCH/hDNA/AuNPs/GCE electrode for 0.5 h at 37 °C, and then 1 U mL^{-1} of UDG was incubated on the electrode to continue incubation for 60 min. Finally, the biosensor was exposed to 10 μL of OAPS-Por/Thi@AuNPs-ssDNA at 37 °C for 60 min and DPV was finally detected.

2.6. Treatment of HeLa cell

The human cervical carcinoma cell line (HeLa cell) was grown in Dulbecco's modified Eagle's medium (DMEM, Invitrogen, USA) supplemented with 10% fetal bovine serum (FBS; Gibco, USA) and 1% penicillin-streptomycin (Gibco, USA), and maintained in a humidified atmosphere (95% air and 5% CO_2) at 37 °C. In the exponential phase of growth, HeLa cells were washed twice with ice-cold PBS (0.1 M, pH 7.4) by centrifugation (1000 rpm, 5 min, 4 °C). Then the cells were resuspended in 100 μL of lysis buffer and kept on ice for 0.5 h. Finally, the supernatant was frozen at -80 °C for further use after centrifugation at 12 000 rpm for 20 min at 4 °C.

3. Results and discussion

3.1. Principle of the UDG detection

Scheme 1 demonstrates the principle of the electrochemical sensor for detecting UDG. A key element of the sensor is OAPS-Por, which can support the electrochemically active substance Thi by a simple adsorption reaction, and also has high electrocatalytic activity towards Thi. Furthermore, two thiol-labelled DNA probes were designed in this work: hDNA and ssDNA. These two DNAs were immobilized on AuNPs/GCE and OAPS-Por/Thi@AuNPs through an Au–S bond, respectively. In addition, the hDNA was modified with four uracil bases. When UDG was present, the uracil bases in hDNA were removed, producing four AP sites, resulting in the release of single-stranded DNA. Subsequently, hDNA hybridized with the ssDNA, leading to the attachment of signal probes on the sensing electrode. When electrochemical measurements were investigated, the signal probe attached to the electrode could generate a pair of peak currents from Thi. In addition, the OAPS-Por

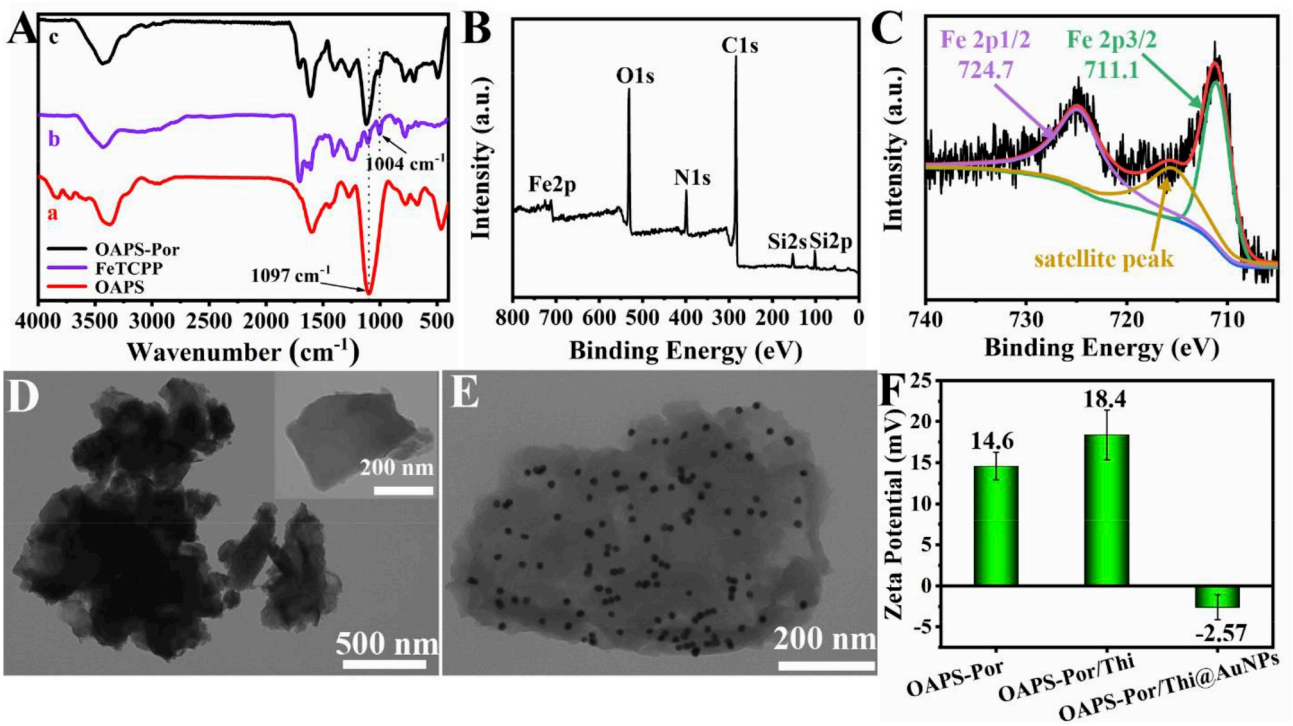

Fig. 1. (A) FT-IR spectra for OAPS, FeTCPP, and OAPS-Por. (B). XPS survey scan of OAPS-Por. (C) High-resolution Fe 2p XPS spectra of OAPS-Por. (D) TEM images of OAPS-Por. Inset: enlarged morphology. (E) TEM image of OAPS-Por/Thi@AuNPs. (F) Zeta potentials of OAPS-Por, OAPS-Por/Thi, and OAPS-Por/Thi@AuNPs.

could electrocatalytically reduce Thi in the electrode surface to further amplify the signal due to the short distance. Thus, the developed sensor can be used to sensitively detect UDG.

3.2. Characteristics of OAPS-Por, OAPS-Por/Thi, and OAPS-Por/Thi@AuNPs

OAPS-Por was synthesized by a condensation reaction between OAPS and FeTCPP (Scheme 1A). The –COOH groups in FeTCPP were first activated by EDC/NHS for 12 h and then OAPS was added. Due to the amidation reaction between carboxylic acid groups of FeTCPP and amino groups of OAPS, OAPS-Por with an extensive polymeric network structure was obtained. The successful fabrication of OAPS-Por was verified by FT-IR and XPS analysis (Fig. 1). As shown in Fig. 1A, the band at 1097 cm^{-1} attribute to the Si–O–Si stretching vibration in OAPS (curve a) (Sun et al., 2018). The band at 1004 cm^{-1} was associated with the Fe–N stretch in FeTCPP (curve b) (Yoo et al., 2015). These two peaks were also appeared in the FT-IR spectrum of OAPS-Por (curve c), clearly identifying the successful combination of FeTCPP with OAPS. This result was also verified by the XPS spectra (Fig. 1B). The survey XPS spectrum showed that C, N, O, Si, and Fe elements existed in OAPS-Por without any other impurities. The high-resolution Fe2p XPS spectrum (Fig. 1C) displayed two peaks at 724.7 and 711.1 eV, which could be assigned to $Fe2p_{1/2}$ and $Fe2p_{3/2}$, respectively, indicating the existence of Fe(III) (Johnson et al., 2018). TEM images showed that the morphology of the synthesized OAPS-Por was irregular schistose morphologies with hundreds of nanometers in length (Fig. 1D). The thermal stability of OAPS-Por was investigated by Thermogravimetric analysis (TGA). OAPS-Por had excellent thermal stability and retaining 90% of the mass at 287 °C (Fig. S1).

OAPS-Por/Thi was obtained by immersing OAPS-Por in the Thi solution with stirring for 24 h. After adsorption equilibrium was reached, the adsorption amount (Q_e) (mg g^{-1}) for Thi was obtained according to Equation: $Q_e=(C_0–C_e)V/m$ (Liu et al., 2018), in which C_0 and C_e (mg L^{-1}) are the initial and equilibrium concentrations of Thi in solution, respectively, V (L) is the volume of the Thi solution, and m (g) is the mass of OAPS-Por. The concentration of residual Thi was obtained using the absorbance at 598 nm of equilibrium solution and standard concentration curve of Thi (Fig. S2). Finally, the results demonstrate that 90.27 mg of Thi can be absorbed onto 1 g of OAPS-Por. In addition, after adsorption, the color of the OAPS-Por/Thi solution was gray blue, which was different from that of OAPS-Por (gray-black) and Thi solution (blue) (Fig. S3).

In order to verify whether OAPS-Por/Thi is electrically active, the cyclic voltammetry (CV) of different electrodes in a pH 5.0 HAc-NaAc solution (Fig. S4). For bare GCE and OAPS-Por/GCE, no redox peaks were observed due to without the electroactive indicator (curve a and b in Fig. S4), while an anodic peak current at -0.12 V and a larger cathodic peak current at around -0.18 V were observed for OAPS-Por/Thi/GCE (curve c), suggesting that Thi had been successfully loaded on the OAPS-Por and can be used as an electroactive indicator. It is noteworthy, that when OAPS-Por was immobilized on the GCE and the same amount of Thi as that loaded on OAPS-Por was put in the HAc-NaAc solution, (curve d), no redox peak of Thi appeared. These results implied that the adsorption caused Thi to be concentrated in OAPS-Por, which greatly reduced the distance between Thi and the electrode and in turn effectively improved the detection sensitivity of the constructed platform.

In order to obtain OAPS-Por/Thi@AuNPs, AuNPs was first prepared. The TEM image (Fig. S5) showed that the prepared AuNPs' diameter was ~19 nm. After being reacted with AuNPs, the surface of OAPS-Por/Thi appeared AuNPs and dispersed uniformly (Fig. 1E), suggesting that AuNPs are successfully interacted with the OAPS-Por/Thi. From the image, it was also proved that the OAPS-Por maintained its original structure after reacting with Thi and AuNPs. Furthermore, we used the zeta potential to record the process of the two reactions. From Fig. 1F, the zeta potential of OAPS-Por in ultra-pure water was 14.6 ± 1.67 mV due to the residual amino groups. After adsorption of positively charged Thi, the zeta potential of OAPS-Por/Thi increased to 18.4 ± 3.06 mV, indicating that Thi was successfully supported on OAPS-Por. Subsequently, the zeta potential of OAPS-Por/Thi@AuNPs changed from

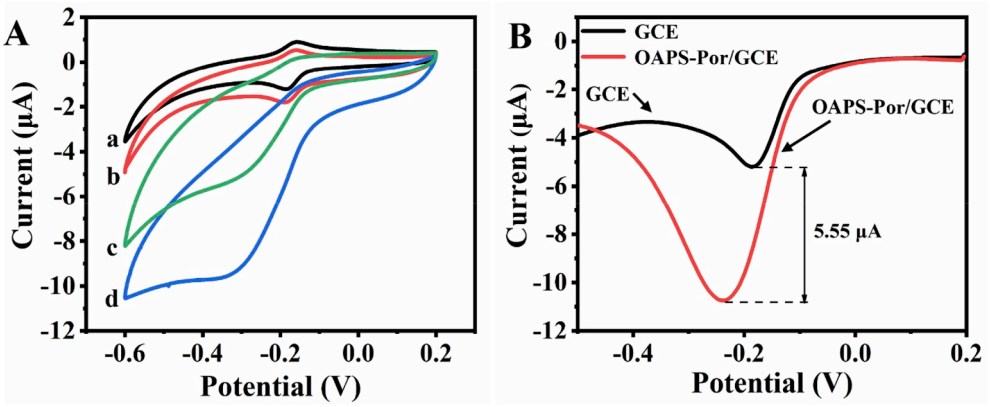

Fig. 2. CVs (A) of GCE (a), OAPS/GCE (b), FeTCPP/GCE (c) and OAPS-Por/GCE (d) and DPVs (B) of GCE and OAPS-Por/GCE in 0.1 M HAc-NaAc buffer (pH 5) including 35 μM Thi.

positive to negative (-2.57 ± 1.51 mV), further identifying the successful coating of negatively charged citrate-capped AuNPs on the surface of OAPS-Por/Thi.

3.3. Electrocatalysis of OAPS-Por

CV and DPV measurements were used to evaluate the electrocatalytic activity of OAPS-Por towards Thi in 0.1 M HAc-NaAc (pH 5.0) containing 35 μM Thi (Fig. 2). OAPS-Por (10 μL, 1 mg mL^{-1}) and equivalent concentration of OAPS and FeTCPP in OAPS-Por were dropped on the GCE and measured after drying under infrared light. From Fig. 2A, the well-defined redox peaks of Thi were observed for bare GCE (curve a) and there was no significant change at OAPS/GCE (curve b), demonstrating that the OAPS had good electrical conductivity and did not hinder the transmission of electrons. However, After FeTCPP was coated on the electrode (curve c), the peak oxidation current decreased, the peak reduction current significantly increased, and the peak reduction potential shifted to a more negative value. Compared with FeTCPP/GCE, OAPS-Por/GCE showed a stronger reduction current (curve d), indicating that OAPS-Por had an obvious electrocatalytic process towards the reduction of Thi, similar to the common horseradish peroxidase (HRP)-H_2O_2 system (Fang et al., 2015; Mani et al., 2009). OAPS-Por had stronger catalytic ability than FeTCPP because loading FeTCPP into the network of OAPS-Por avoided the self-degradation of the porphyrins and the formation of μ-oxide dimers. The electrocatalytic activity of OAPS-Por towards the reduction of Thi was clearer in DPV (Fig. 2B). Compared with GCE, the cathodic peak shifted left, from -0.188 to -0.24 V, and cathodal current value improved by 5.55 μA when OAPS-Por was immobilized on GCE.

In addition, the influence of temperature on electrocatalytic property of OAPS-Por and HRP-H_2O_2 system were investigated. OAPS-Por and HRP incubated in the range from 0 to 100 °C for 120 min were coated on electrodes, and investigated in a 35 μM Thi solution (pH 5.0, containing 1 mM H_2O_2 for HRP), respectively. As shown in Fig. S6, HRP maintained good catalytic activity under low temperature (0–40 °C) but quickly decreased with the variation of temperature from 40 to 100 °C. In contrast, the OAPS-Por was hardly affected by temperature. When the temperature reached 100 °C, the catalytic activity was still maintained at about 90%. Thus, OAPS-Por showed a robustly catalytic performance than HRP, demonstrating it did not require strict storage and operate conditions, which is significant for its practical application.

3.4. Characterizations of the biosensor

To confirm the successful preparation of the sensor, the CV and electrochemical impedance spectroscopy (EIS) were carried out in 0.1 M KCl including 5 mM $K_3[Fe(CN)_6]/K_4[Fe(CN)_6]$ (1:1). From Figs. S7A and a well-defined redox peak of $[Fe(CN)_6]^{3-/4-}$ at the bare electrode could be observed (curve a). Upon AuNPs was electrodeposited on the electrode surface (curve b), the current was obviously increased, because AuNPs can enhance the electron transfer rate. After incubating with hDNA on AuNPs/GCE, the signal response reduced (curve c), owing to the electrostatic repulsion between negative charges of DNA and Fe $(CN)_6^{3-}/^{4-}$, inhibited the electron transfer. Subsequently, when hDNA/AuNPs/GCE was modified with MCH (curve d), a decline was exhibited, and this can be ascribed to the fact that MCH blocked electron transfer rate. Nevertheless, when OAPS-Por/Thi@AuNPs-ssDNA was incubated with the electrode after the incubation of UDG (1 U mL^{-1}), the current interestingly increased (curve e), which indicated that the OAPS-Por/Thi@AuNPs-ssDNA successfully interacted with hDNA on the electrode and the synthesized OAPS-Por/Thi@AuNPs-ssDNA possessed good electron transfer efficiency, although ssDNA acted as a barrier to insulate the transference of the electrons. The above results indicated the successful fabrication of the biosensor for UDG detection. The EIS results (Fig. S7B) were consistent with that of CV, further confirming that AuNPs, hDNA, MCH, and OAPS-Por/Thi@AuNPs-ssDNA were successfully assembled on the electrode surface step by step.

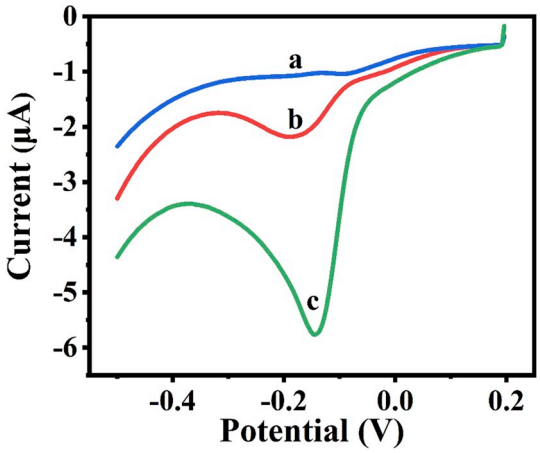

Fig. 3. DPV responses of MCH/hDNA/AuNPs/GCE (a), and MCH/hDNA/AuNPs/GCE after incubation with OAPS-Por/Thi@AuNPs-ssDNA in the absence of UDG (b) and in the presence of UDG (c) in the NaAc-HAc buffer solution (pH 5.0). UDG concentration: 0.25 U mL^{-1}.

3.5. Feasibility of the biosensor

The feasibility of the biosensor was identified and the results were present in Fig. 3. MCH/hDNA/AuNPs/GCE showed no DPV peak current

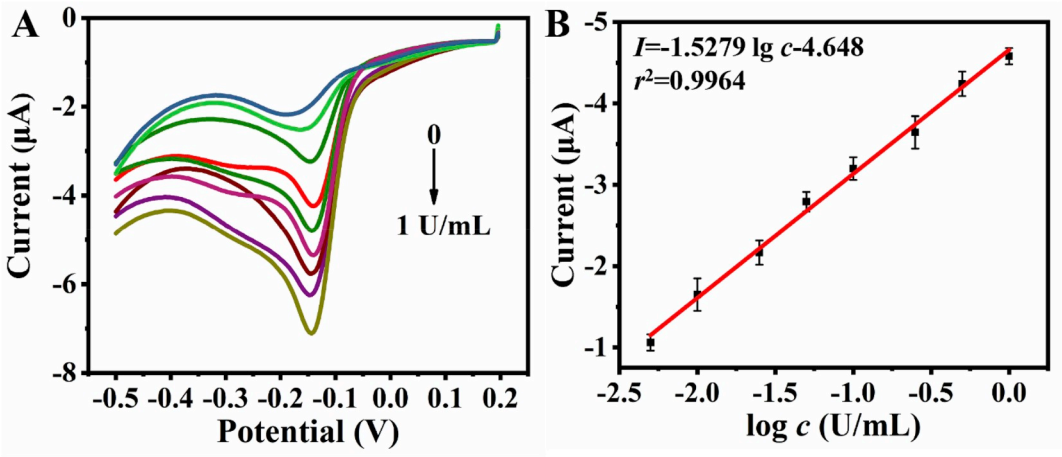

Fig. 4. (A) DPV responses of OAPS-Por/Thi@AuNPs-ssDNA to different concentrations of UDG: 0, 0.005, 0.01, 0.025, 0.05, 0.1, 0.25, 0.5, and 1 U mL^{-1} (from top to bottom) in 0.1 M HAc-NaAc buffer (pH 5.0). (B) The calibration plot of peak current and the logarithm of UDG concentrations.

due to the absence of a detectable electroactive indicator (curve a). When MCH/hDNA/AuNPs/GCE was incubated with UDG (0.25 U mL^{-1}) and next incubated with OAPS-Por/Thi@AuNPs-ssDNA, a strong peak at −0.15 V was observed (curve c). This result should correspond to that of the removal of the four uracil bases from hDNA by UDG, resulting in the hairpin structure opened, and then the latter could bind with OAPS-Por/Thi@AuNPs-ssDNA, which generated a DPV peak current from Thi as a detectable electrochemical indicator and also OAPS-Por could effectively electrocatalytic oxidation of Thi to further amplify this signal. In the absence of UDG, only a very weak peak was observed owing to the nonspecific interaction between signal probe and the electrode (curve b).

3.6. Optimization of the detection conditions

To display an electrochemical sensor with high sensitivity towards UDG, experimental conditions such as the hDNA immobilization concentration, the incubation time of UDG, and the hybridization time of OAPS-Por/Thi@AuNPs-ssDNA with hDNA were investigated. The result revealed that with an increasing hDNA concentration, the peak reduction current gradually upgraded to 0.5 μM and then slowly declined at higher concentrations, possibly because the increased steric hindrance hindered the combination of hDNA and ssDNA (Fig. S8A). Therefore, 0.5 μM was regarded as the best hDNA concentration. To our knowledge, incubation time between UDG and hDNA is another identically crucial parameter associated with the final hybridization and electrochemical detection. To ensure a maximal amplified response, the effect of incubation time between UDG and hDNA was studied (Fig. S8B). The peak current values increased with time and tended to steady after 1 h. Therefore, 1 h was regarded as the optimised time for the incubation of UDG. In addition, the hybridization time between OAPS-Por/Thi@AuNPs-ssDNA and hDNA was investigated (Fig. S8C). After a hybridization time of 60 min, the peak current reached a plateau. Thus, 60 min was selected as the optimized hybridization time between OAPS-Por/Thi@AuNPs-ssDNA and hDNA.

3.7. Detection of UDG activity

Under optimal experimental conditions, the fabricated biosensor was used to quantitatively detect UDG with DPV measurements (Fig. 4A). The responses of peak cathode current proportionally raised with the increasing UDG concentration. A well linear correlation was obtained between peak currents and the logarithm of UDG concentrations, ranging from 0.005 to 1 U mL^{-1} (Fig. 4B). The linear regression equation was expressed as I = -1.5279 lg c-4.648 (R^2 = 0.9964) with a detection limit of 6.97 × 10^{-4} U mL^{-1} (S/N = 3). Notably, the proposed method exhibited a wider linear range and higher sensitivity than other related reports (Table S1). The electrochemical performance of the biosensor has been improved which would attribute to following aspects: (1) The large surface area of OAPS-Por guarantied the loading of more Thi for generating a stronger signal and AuNPs for connecting more ssDNA. (2) AuNPs uniformly dispersed on OAPS-Por improves the signal transduction capability to the surface electrode. (3) The good electrocatalytic activity of OAPS-Por towards Thi generates an enhanced signal without H_2O_2. (4) The efficient cleavage of hDNA by UDG. (5) The signal molecule is attached to the electrode as a probe, not in solution, thus greatly reducing the background signal.

3.8. Selectivity, repeatability and stability of the designed platform

To monitor the specificity of the proposed strategy, other DNA glycosylases including Fpg, hAAG, and an irrelevant protein (bovine serum albumin, BSA) were analyzed under the same conditions (Fig. S9). When the biosensor was incubated with BSA, Fpg, and hAAG solutions, respectively, no obvious signal was observed, similar to blank sample. However, the peak current was significantly enhanced when UDG was existed in the system, implying that the established biosensor exhibited good selectivity. The repeatability of the strategy was next investigated. Firstly, the same batch of prepared electrodes (MCH/hDNA/AuNPs/GCE) and the same batch of signal probe (OAPS-Por/Thi@AuNPs-ssDNA) were utilized for the assay. The relative standard deviations (RSD) were 2.5% and 3.5% at 0.025 U mL^{-1} and 0.05 U mL^{-1} of UDG, respectively (Table S2). At the same time, the different batch of prepared electrodes and signal probes were also used for the assay in six days. The RSDs of different batch were 4.3% and 5.2% at 0.025 U mL^{-1} and 0.05 U mL^{-1}, respectively (Table S3). The results clearly implied the high repeatability of the fabricated biosensor. Finally, the stability of the biosensor was studied. The constructed electrodes were placed at 4 °C and evaluated every 5 days. The current signal can still retain 91.4% of its initial response after 20 days (Fig. S9B). The result demonstrated that our biosensor exhibits long term stability, which is mainly due to the stability of OAPS-Por.

3.9. Inhibition of the UDG assay

UDG can prevent DNA-damage and maintain genomic integrity. However, investigation revealed that UDG activity could decrease the therapeutic efficiency of chemotherapeutic drugs for DNA-damage (Benjamin and Wadih, 2010). Therefore, an assay of the inhibition of UDG was also investigated by this proposed electrochemical

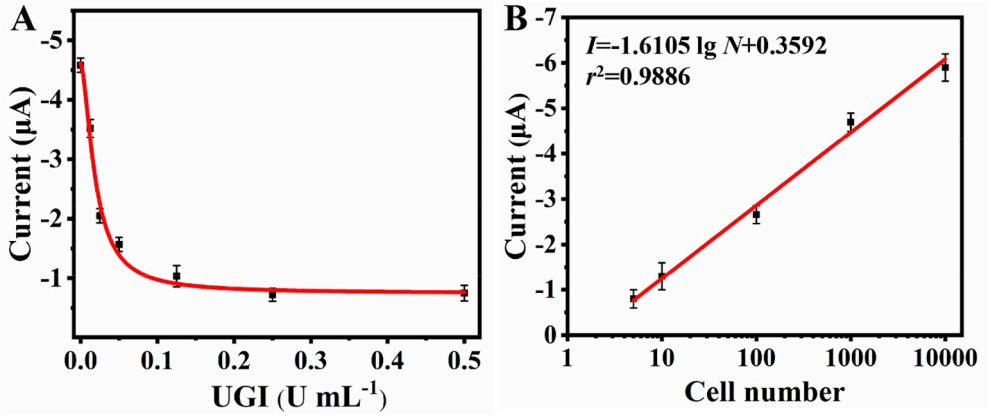

Fig. 5. (A) DPV responses of the biosensor in the presence of various UGI concentration (0.0125, 0.025, 0.05, 0.125, 0.25, and 0.5 U mL^{-1}). The UDG concentration was 1 U mL^{-1}. (B) The calibration plot of peak current and the logarithm of cell number.

amplification strategy. UGI was used as a model inhibitor in the present investigation. UGI was extracted from the subtilis bacteriophage PBS1, and can inhibit UDG activity by forming close-knit and physiologically irreversible complexes with a 1:1 (UDG:UGI) stoichiometry (Kaushal et al., 2010). From Fig. 5A, the peak current decreased when the concentrations of UGI increased. The half maximal inhibitory concentration (IC_{50}) obtained was 0.03 U mL^{-1}, which is consistent with previous report (Lee et al., 2015). UDG activity was almost completely inhibited when the UGI concentration was elevated to 0.5 U mL^{-1}. The results indicated that the developed biosensor can be used for measurement of UDG inhibitors.

3.10. The UDG assay in real samples

To investigate the feasibility of the proposed biosensor in real and complex sample, we detected the UDG activities in HeLa cells and human blood serums. As can be seen in Fig. 5B, with an increasing number of HeLa cells, DPV peak current was significantly enhanced, which is ascribed to the presence of UDG. On logarithmic scale, the peak currents showed the corresponding linear relationship with the HeLa cell number ranging from 5 to 10000 cells. The regression equation is I = -1.6105 lg N+0.3592 and the correlation coefficient is 0.9886. The detection limit of 2 cells was determined at S/N = 3. Meantime, according to the linear correlation equation, the UDG activity in HeLa cell lysate was obtained to be 0.062 U mL^{-1}. This, in combination with the sum total protein in HeLa lysate (0.25 mg mL^{-1}), measured via a BCA protein assay kit, the UDG activity was calculated as 0.25 U per 1 mg total protein, approximating to the previous reports (Du et al., 2018; Tao et al., 2015; Wu et al., 2016). Next, the recoveries of different concentration of UDG in HeLa cells and 5% human blood serum samples were measured by standard addition method. The recoveries of proposed biosensor were in the range of 96.7%–102.5% (RSD = 1.7%–3.8%) for Hela cells and 98.0%–107.4% (RSD = 2.9%–4.3%) for human blood serums, respectively (Table S4 and Table S5). These results demonstrated that the proposed strategy possesses reliable potential utility for UDG detection in clinical application.

4. Conclusions

In summary, we successfully fabricated a novel nanomaterial (OAPS-Por)-based electrochemical biosensor to detect UDG activity sensitively. The analysis process was based on the principle that the hDNA unfolded in the presence of UDG, and the signal probes were connected on the electrode surface, leading the signal current readout. The OAPS-Por could not only absorb much Thi, but also possess obvious electrocatalytic activity toward the reduction of Thi without involvement of H_2O_2, which enhanced the electrochemical signal. Meantime, not involving H_2O_2 effectively improved the stability and sensitivity. Under optimal conditions, the biosensor exhibited satisfactory sensitivity (LOD = 6.97×10^{-4} U mL^{-1}) and a wide range from 0.005 to 1 U mL^{-1}, which is superior to the other reported methods for UDG detection. Moreover, the platform was used to monitor UDG inhibitor and UDG in HeLa cell lysates and human blood serums, proving that the substrate-free biosensor has great prospect in clinical diagnostics and biomedical research.

Declaration of competing interest

The authors declare that they have no known competing financial interests or personal relationships that could have appeared to influence the work reported in this paper.

CRediT authorship contribution statement

Tingting Liu: Conceptualization, Investigation, Writing - original draft. **Lin Cui:** Conceptualization, Writing - review & editing. **Dekang Li:** Software. **Wenqiang Gao:** Data curation. **Lili Wu:** Writing - review & editing. **Xiaomei Zhang:** Conceptualization, Writing - review & editing, Supervision.

Acknowledgements

This work was supported by the National Natural Science Foundation of China (21977064, 21472117, 21605096), the Fundamental Research Funds of Shandong University (2018JC036) and Open Project of State Key Laboratory of Infrared Physics (M201701). Thanks to Dr. Edward C. Mignot, Shandong University, for linguistic advice.

Appendix A. Supplementary data

Supplementary data to this article can be found online at https://doi.org/10.1016/j.bios.2020.112014.

References

Benjamin, J.M., Wadih, A.A.R.P., 2010. Curr. Drug Targets 11, 1336–1340.
Chen, L., Yang, Y., Jiang, D., 2010. J. Am. Chem. Soc. 132, 9138–9143.
Cui, L., Hu, J., Li, C., Wang, C., Zhang, C., 2018. Biosens. Bioelectron. 122, 168–174.
Cui, L., Wang, M., Sun, B., Ai, S., Wang, S., Zhang, C., 2019. Chem. Commun. 55, 1172–1175.
David, S.S., Williams, S.D., 1998. Chem. Rev. 98, 1221–1262.
David, S.S., O'Shea, V.L., Kundu, S., 2007. Nature 447, 941–950.
Di Noia, J., Neuberger, M.S., 2002. Nature 419, 43–48.
Du, Y., Jiang, H., Huo, Y., Han, G., Kong, D., 2016. Biosens. Bioelectron. 77, 971–977.
Du, Y., Cui, Y., Li, X., Sun, G., Zhang, Y., Tang, A., Kim, K., Kong, D., 2018. Anal. Chem. 90, 8629–8634.
Fang, Y., Huang, X., Wang, L., Wang, J., 2015. Biosens. Bioelectron. 64, 324–332.

Ghanbari, H., Cousins, B.G., Seifalian, A.M., 2011. Macromol. Rapid Commun. 32, 1032–1046.
Jiao, F., Qian, P., Qin, Y., Xia, Y., Deng, C., Nie, Z., 2016. Talanta 147, 98–102.
Johnson, E.M., Haiges, R., Marinescu, S.C., 2018. ACS Appl. Mater. Interfaces 10, 37919–37927.
Kaushal, P.S., Talawar, R.K., Krishna, P.D., Varshney, U., Vijayan, M., 2010. Acta Crystallogr. 64, 551–560.
Lee, C.Y., Park, K.S., Park, H.G., 2015. Chem. Commun. 51, 13744–13747.
Li, C., Zhang, Y., Tang, B., Zhang, C., 2018. Chem. Commun. 54, 5839–5842.
Liao, W., Yang, S., Hsiao, S., Wang, Y., Li, S., Ma, C.M., Tien, H., Zeng, S., 2014. ACS Appl. Mater. Interfaces 6, 15802–15812.
Lin, S., Diercks, C.S., Zhang, Y., Kornienko, N., Nichols, E.M., Zhao, Y., Paris, A.R., Kim, D., Yang, P., Yaghi, O.M., Chang, C.J., 2015. Science 349, 1208.
Ling, P., Lei, J., Ju, H., 2016. Anal. Chem. 88, 10680–10686.
Ling, P., Lei, J., Zhang, L., Ju, H., 2015. Anal. Chem. 87, 3957–3963.
Liu, Q., Liu, C., Zhu, G., Xu, H., Zhang, X.J., Hu, C., Xie, Y., Zhang, K., Wang, H., 2019. Microchim. Acta 186, 179.
Liu, T., Jing, L., Cui, L., Liu, Q., Zhang, X., 2018. Chemosphere 212, 1038–1046.
Liu, T., Tian, J., Cui, L., Liu, Q., Wu, L., Zhang, X., 2019. Colloids Surf., B 178, 137–145.
Liu, X., Chen, M., Hou, T., Wang, X., Liu, S., Li, F., 2013. Electrochim. Acta 113, 514–518.
Mani, V., Chikkaveeraiah, B.V., Patel, V., Gutkind, J.S., Rusling, J.F., 2009. ACS Nano 3, 585–594.
Nagai, A., Chen, X., Feng, X., Ding, X., Guo, Z., Jiang, D., 2013. Angew. Chem. Int. Ed. 52, 3770–3774.
Nc, D.S.P., Harris CCBohr, V.A., 2004. Oncogene 23, 6559–6568.
Schärer, O.D., 2003. Angew. Chem. Int. Ed. 42, 2946–2974.
Seal, G., Brech, K., Karp, S.J., Cool, B.L., Sirover, M.A., 1988. Proc. Natl. Acad. Sci. U.S.A. 85, 2339–2343.
Sousa, M.M.L., Krokan, H.E., Slupphaug, G., 2007. Mol. Asp. Med. 28, 276–306.
Sun, R., Feng, S., Wang, D., Liu, H., 2018. Chem. Mater. 30, 6370–6376.
Tao, J., Song, P., Sato, Y., Nishizawa, S., Teramae, N., Tong, A., Xiang, Y., 2015. Chem. Commun. 51, 929–932.
Wang, J., Pan, M., Wei, J., Liu, X., Wang, F., 2017. Chem. Commun. 53, 12878–12881.
Wang, Q., Lei, J., Deng, S., Zhang, L., Ju, H., 2013. Chem. Commun. 49, 916–918.
Wang, X., Chrzanowski, M., Yuan, D., Sweeting, B.S., Ma, S., 2014. Chem. Mater. 26, 1639–1644.
Wei, J., Gong, X., Wang, Q., Pan, M., Liu, J., Xia, F., Wang, F., 2018. Chem. Sci. 9, 52–61.
Wu, Y., Wang, L., Zhu, J., Jiang, W., 2015. Biosens. Bioelectron. 68, 654–659.
Wu, Y., Yan, P., Xu, X., Jiang, W., 2016. Analyst 141, 1789–1795.
Wu, Z., Chen, L., Liu, J., Parvez, K., Liang, H., Shu, J., Sachdev, H., Graf, R., Feng, X., Müllen, K., 2014. Adv. Mater. 26, 1450–1455.
Xiang, Z., Xue, Y., Cao, D., Huang, L., Chen, J., Dai, L., 2014. Angew. Chem. Int. Ed. 53, 2433–2437.
Xue, T., Jiang, S., Qu, Y., Su, Q., Cheng, R., Dubin, S., Chiu, C., Kaner, R., Huang, Y., Duan, X., 2012. Angew. Chem. Int. Ed. 51, 3822–3825.
Yoo, J., Park, N., Park, J.H., Park, J.H., Kang, S., Lee, S.M., Kim, H.J., Jo, H., Park, J., Son, S.U., 2015. ACS Catal. 5, 350–355.
Zhang, Z., Xue, Y., Zhang, P., Müller, A.H.E., Zhang, W., 2016. Macromolecules 49, 8440–8448.
Zheng, T., Zhang, Q., Feng, S., Zhu, J., Wang, Q., Wang, H., 2014. J. Am. Chem. Soc. 136, 2288–2291.
Zheng, Y., Yuan, Y., Chai, Y., Yuan, R., 2015. Biosens. Bioelectron. 66, 585–589.